minerals

MDPI

Article

Discrimination of Mineralization Types of Skarn Deposits by Magnetite Chemistry

Huan Xie [1,2], Xiaowen Huang [1,*], Yumiao Meng [1], Houmingrui Tan [1,2] and Liang Qi [1]

[1] State Key Laboratory of Ore Deposit Geochemistry, Institute of Geochemistry, Chinese Academy of Sciences, Guiyang 550081, China; xiehuan@mail.gyig.ac.cn (H.X.); mengyumiao@mail.gyig.ac.cn (Y.M.); tanhoumingrui@mail.gyig.ac.cn (H.T.); qilianghku@hotmail.com (L.Q.)

[2] College of Earth and Planetary Science, University of Chinese Academy of Sciences, Beijing 100049, China

* Correspondence: huangxiaowen@vip.gyig.ac.cn

Abstract: There are different mineralization types for skarn deposits with various origins and ore-forming conditions. Magnetite is one of the main ore minerals in skarn deposits, but whether chemical compositions of magnetite can be used to discriminate different mineralization types remains unknown. This paper collects the published magnetite electron probe microanalysis (EPMA) and laser ablation inductively coupled plasma mass spectrometry (LA-ICP-MS) data of skarn deposits and investigates the relationship between magnetite geochemistry and mineralization types of skarn deposits using the partial least squares-discriminant analysis (PLS-DA). For EPMA data, magnetite from Fe-Zn skarn deposits can be roughly separated from that of Cu-Fe-Pb-Zn, Fe, Fe-Co-Bi-Ag, Fe-Cu, and Fe-Zn-Pb skarn deposits due to the relative enrichment of Al and Mn for the former. For LA-ICP-MS data, magnetite from Fe-Sn, Fe-Zn, and W-Mo-Pb-Zn-Fe-Cu skarn deposits can be roughly separated from that of other skarn deposits due to positive correlation with Mn, Zn, and Sn and the negative correlation with V for the former. The relative depletion of V for these mineralization types likely reflects higher oxygen fugacity than the other types of skarn deposits. Magnetite from Fe-Au skarn deposits is separated due to the relatively high Cr and Ga contents, whereas magnetite from Fe-Cu skarn deposits can be discriminated because of the relative enrichment of Mg and Co. The discrimination between different types of skarn deposits in the plot of Mg + Mn vs. (Si + Al)/(Mg + Mn) indicates that the chemical composition of magnetite is significantly affected by the fluid–rock interaction, where magnetite from Fe-Au skarn deposit shows the lowest fluid–rock ratios. The PLS-DA discrimination based on LA-ICP-MS data is better than that of EPMA data, and the main discriminant elements for the different mineralization types are Mg, Al, Ti, V, Mn, Co, Zn, Ga, and Sn. Based on the discriminant elements, we propose a plot of Mg+Mn vs. Ga+Sn to discriminate different mineralization types of skarn deposits.

Keywords: mineralization types; skarn deposits; magnetite; discrimination; PLS-DA

Citation: Xie, H.; Huang, X.; Meng, Y.; Tan, H.; Qi, L. Discrimination of Mineralization Types of Skarn Deposits by Magnetite Chemistry. *Minerals* **2022**, *12*, 608. https://doi.org/10.3390/min12050608

Academic Editor: Evgeny Galuskin

Received: 15 April 2022
Accepted: 9 May 2022
Published: 11 May 2022

1. Introduction

Metal deposits that contain skarn as gangue are termed skarn deposits [1]. Skarn deposits can be divided into seven types based on the main metals, i.e., Fe, Au, Cu, Zn, W, Mo, and Sn skarn deposits [2,3]. Previous studies have shown that variations in magmatic compositions and the oxygen fugacity of intrusions cause various types of skarn mineralization [2,4]. It was proposed that the magmatic differentiation degree of related intrusions of Sn and Mo skarn deposits is higher than that of Fe and Au skarn deposits [2]. Compared with the average oxygen fugacity for all intrusions associated with skarns, Au and Sn skarn intrusions are more reduced, while Cu, Zn, and Mo skarn intrusions are more oxidized [2].

Magnetite is one of the main ore minerals in different types of skarn deposits. Magnetite has been used in research on the ore-forming process and mineral exploration [5–9].

A previous study demonstrated that hydrothermal magnetite from magnesian skarn is relatively rich in Mg and Mn and depleted in Al, Ti, Cr, Co, Ni, and Ga, whereas that from calcic skarn has relatively high Mg, Al, Cr, Mn, Co, Ni, and Zn and low Sn contents [6]. It was found that magnetite from Cu-Fe-Au and Fe skarn deposits has different chemical compositions [9]. Magnetite from Fe skarn deposits has a similar Ti + V content but higher Ca + Al + Mn content compared with Cu-Fe-Au skarn deposits, and magnetite from skarn deposits defines a wider compositional range than previously thought in the Ti + V vs. Ca + Al + Mn plot [9]. In addition to magnetite, garnet from different types of skarn deposits also has various compositions [10,11]. Garnet in W-Sn skarn deposits has a relatively high Sn content, whereas that in W-Mo and Cu skarn deposits has relatively high W and V contents, respectively [11]. These studies show that different types of skarn deposits are formed in different geological environments, which can be recorded by mineral chemistry. However, due to the limited data, the differences in the chemical composition of minerals such as magnetite are not well-illustrated, and thus, the specific controlling factors leading to the formation of different types of skarn deposits remain a matter of debate. Moreover, the discrimination between different types of skarn deposits needs to be constructed based on a large dataset.

In this study, we summarize the published electron probe microanalysis (EPMA) and laser ablation inductively coupled plasma mass spectrometry (LA-ICP-MS) data of magnetite from skarn deposits worldwide. These data are investigated by partial least squares-discriminant analysis (PLS-DA) to constrain the factors controlling the various chemistry of magnetite from different mineralization types. A plot of Mg + Mn vs. Ga+Sn is proposed to discriminate different types of skarn deposits and can be used for the identification of magnetite with unknown origins.

2. Data and Analytical Methods

2.1. Data Preparation

We collected magnetite EPMA and LA-ICP-MS data from a total of 50 skarn deposits worldwide (Figure 1). Most skarn deposits were distributed in China, with five from British Columbia, Canada, four from Peru, five from the Loei Fold Belt, Thailand, two from Mongolia, one from Romania, and one from Siberia. The EPMA data contained 894 analyses of 6 mineralization types (Cu-Fe-Pb-Zn, Fe, Fe-Co-Bi-Ag, Fe-Cu, Fe-Zn, and Fe-Zn-Pb), whereas the LA-ICP-MS data contained 1289 analyses of 9 mineralization types (Cu-Fe-Au, Fe, Fe-Au, Fe-Cu, Fe-Mo, Fe-Sn, Fe-Zn, Fe-Zn-Pb, and W-Mo-Pb-Zn-Fe-Cu). The number and proportion of the data for different mineralization types are shown in Figure 2. The main mineralization types are Fe deposits with magnetite EPMA and LA-ICP-MS data accounting for 47.7% and 41.7%, respectively (Figure 2). In addition, the detailed information about the collected skarn deposits, including the deposit name, location, the composition of the intrusions and host rocks, and the data source, are shown in Supplementary Material Table S1.

2.2. Statistical Methods

The magnetite EPMA and LA-ICP-MS data were investigated by the multivariate statistical method PLS-DA to reveal the key factors controlling different mineralization types of skarn deposits. The data preprocessing was similar to the work done by Huang et al. (2019) [12]. The proportions of the censored data for EPMA and LA-ICP-MS are shown in Table S2. Elements with censored values $\leq$ 40% were used for the PLS-DA, so there were 5 elements (Mg, Al, Si, Ti, and Mn) analyzed by EPMA and 13 elements (Mg, Al, Si, Ca, Ti, V, Cr, Mn, Co, Ni, Zn, Ga, and Sn) analyzed by LA-ICP-MS used as the discriminant analysis. The robCompositon package in R software was used to interpolate the data of the elements whose censored data were less than 40%. In order to overcome the closure of the concentration data, the centered logarithm ratio was used for data conversion.

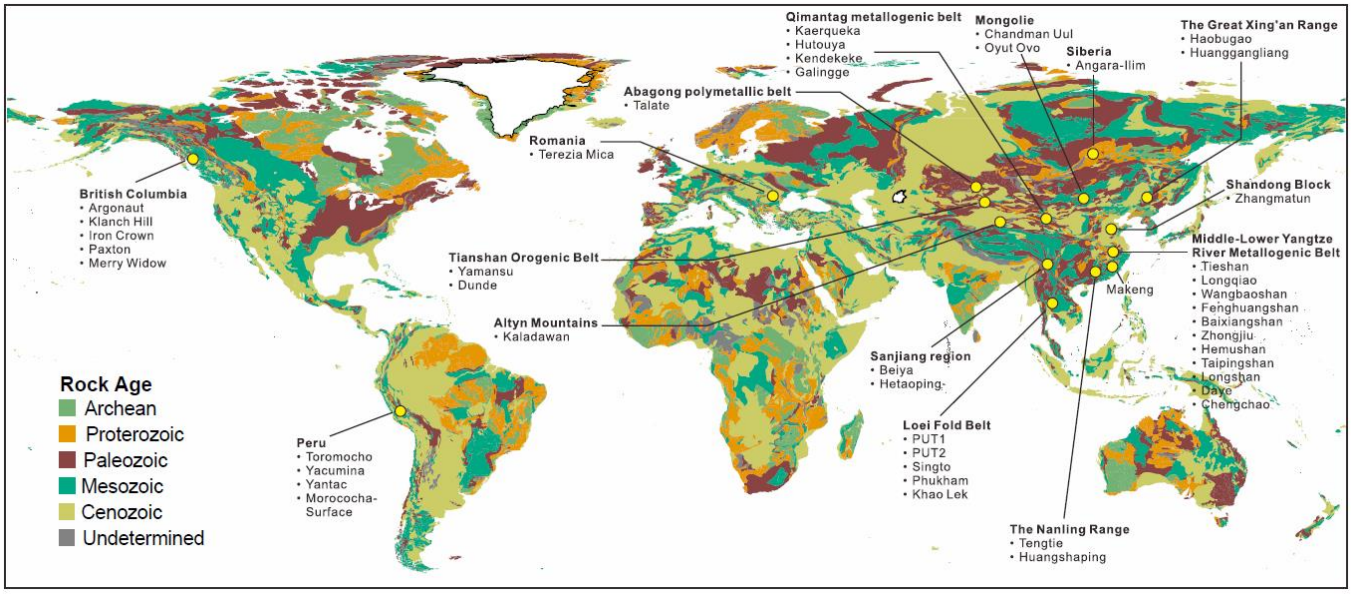

Figure 1. Distribution of the skarn deposits collected in this study. The physical map of world is from M. Colpron (Geological Survey of Canada, Ottawa, ON, Canada).

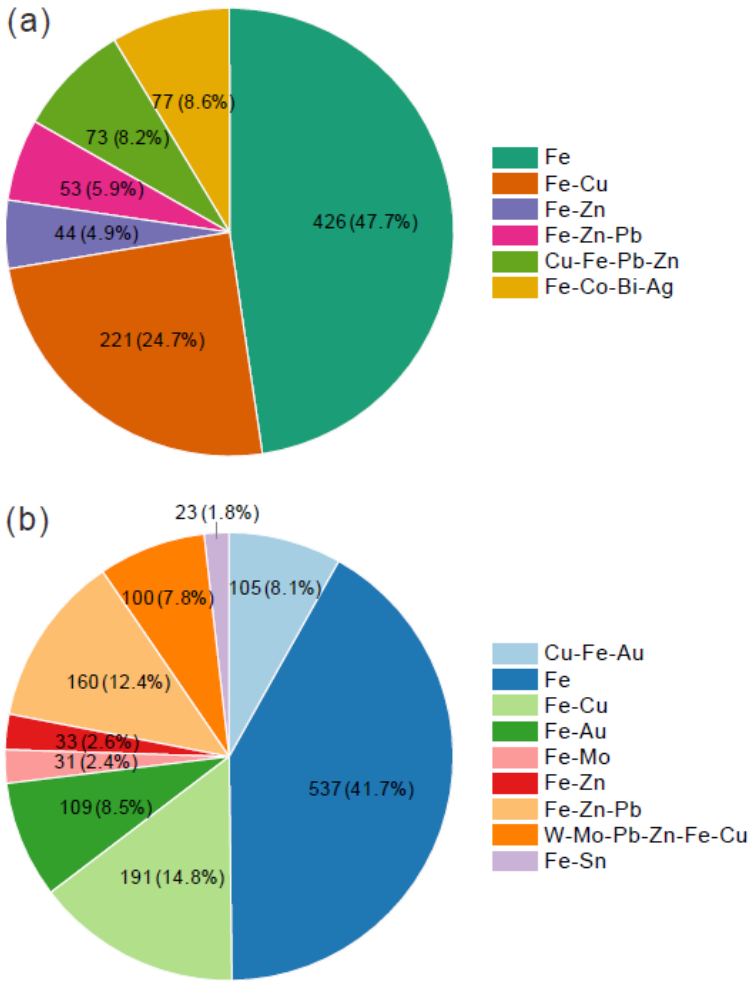

Figure 2. Number and proportion of EPMA (**a**) and LA-ICP-MS (**b**) data of magnetite from different mineralization types of skarn deposits. Nearly half of the data are from Fe skarn deposits.

Partial least squares-discriminant analysis is a supervised multivariate statistical method. The goal of PLS-DA is to strengthen the separation between the observation groups by rotating the principal components so as to obtain the maximum separation between classes and to understand which variables carry class separation information [13,14]. The PLS-DA component is extracted in decreasing order of importance, and the first two or three components are usually selected to explain the data. PLS-DA score scatter plots (e.g., t_1-t_2) show the distribution of samples in different groups. Score contribution histograms further illustrate the compositional differences in each group, where positive or negative values for an element indicate the relative enrichment or depletion of that element compared to the mean of the dataset. Variance Importance Projection (VIP) graphs characterize the ability of each element in the classification. The elements with VIP values > 1 have the greatest impact on classification, those with VIP values between 0.8 and 1 represent moderately influential variables, and those with VIP values less than 0.8 are less important [7].

3. Results

3.1. Chemical Composition of Magnetite

For EPMA data, the median Mg contents vary from 10^2 to 10^4 ppm, the median Al contents are 10^3 ppm, and the median Si and Ti contents are 10^2 ppm, whereas the median Mn contents vary from 10^2 to 10^3 ppm (Figure 3a). Magnetite from Fe-Zn-Pb and Fe-Co-Bi-Ag skarn deposits have higher median Mg contents than other mineralization types (Figure 3a). Magnetite from Fe-Zn and Fe-Zn-Pb skarn deposits is characterized by a relatively high Al content, whereas magnetite from Fe-Co-Bi-Ag skarn deposits has a relatively high Ti content. Magnetite from Fe and Fe-Cu skarn deposits has a lower Mn content than other mineralization types.

For LA-ICP-MS data, the median Mg, Al, Si, Ca, Ti, and Mn contents vary from 10^2 to 10^4 ppm; the median Cr, Co, Ni, and Ga contents vary from 10^{-1} to 10^1 ppm; the median V contents vary from 0 to 10^2 ppm; and the median Zn contents vary from 10^1 to 10^3 ppm, whereas the median Sn contents vary from 10^{-1} to 10^3 ppm (Figure 3b). Magnetite from Cu-Fe-Au skarn deposits has relatively high median Si, Ca, Co, and Ga contents. Magnetite from Fe skarn deposits shows higher median Mg, Ti, V, and Co contents. Magnetite from Fe-Au skarn deposits has relatively high median Si, Cr, and Ga contents. Magnetite from Fe-Cu skarn deposits is characterized by relatively high median Mg, Al, Ti, V, Co, and Ni contents. Magnetite from Fe-Mo skarn deposits has relatively high median Cr but low Ga contents. Magnetite from Fe-Sn skarn deposits shows relatively high median Ti and Zn contents. Magnetite from Fe-Zn skarn deposits is relatively rich in Mn and Sn but depleted in V. Magnetite from Fe-Zn-Pb skarn deposits shows higher median Ca but lower Sn contents than the other mineralization types. Magnetite from W-Mo-Pb-Zn-Fe-Cu skarn deposits has relatively high median Al, Mn, Ni, Zn, and Sn contents (Figure 3b).

Based on the compositions of the skarns, the studied magnetite samples analyzed by EPMA can be divided into Ca and Mg skarns. The EPMA data showed that Ca skarn magnetite is relatively rich in Al and V, whereas Mg skarn magnetite is relatively rich in Si and Mn (Figure 4). There was no significant difference in the Mg, Ca, Co, and Zn contents of magnetite from the Ca and Mg skarns.

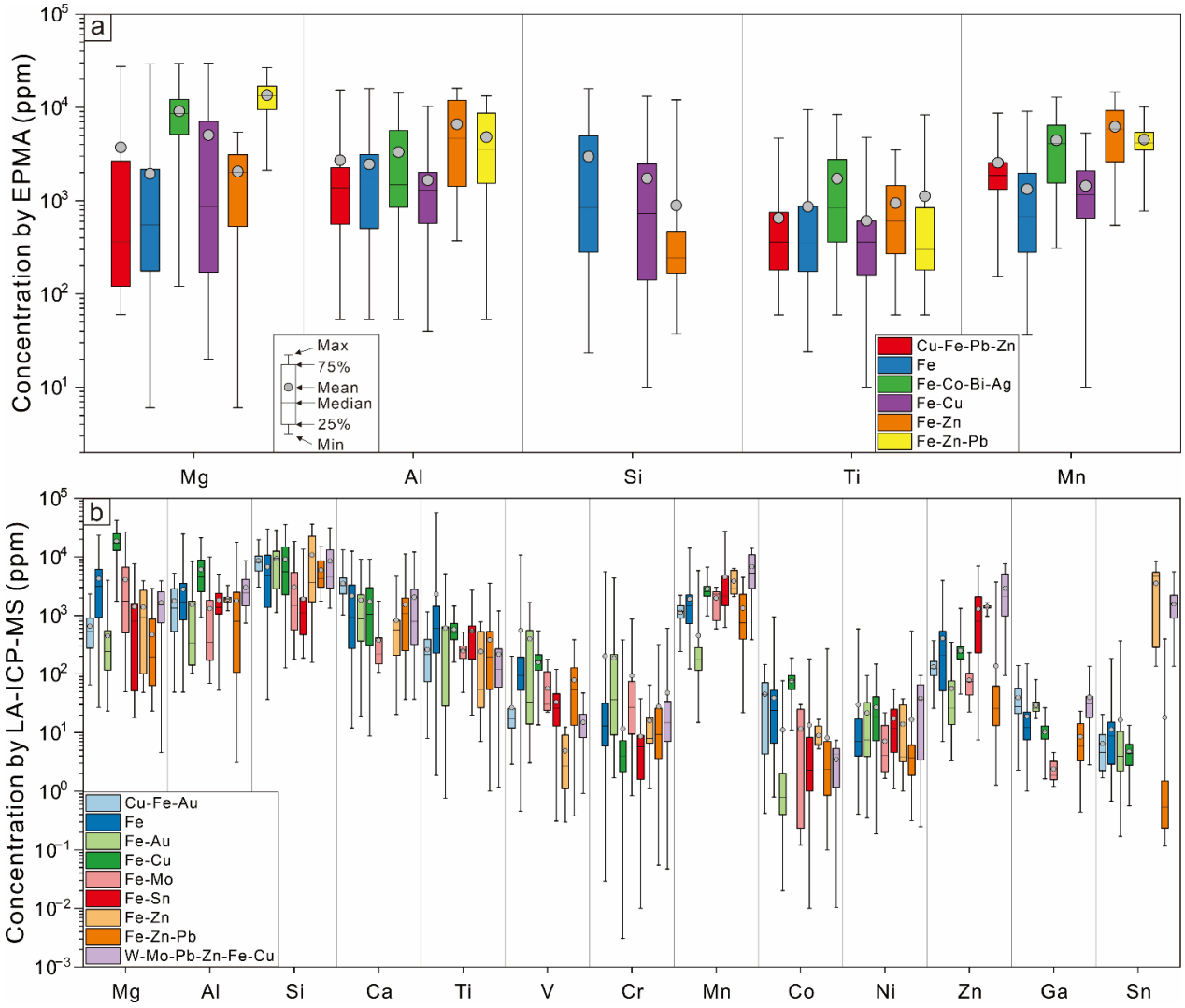

Figure 3. Box and whisker plots showing EPMA (**a**) and LA-ICP-MS; (**b**) trace element contents of magnetite.

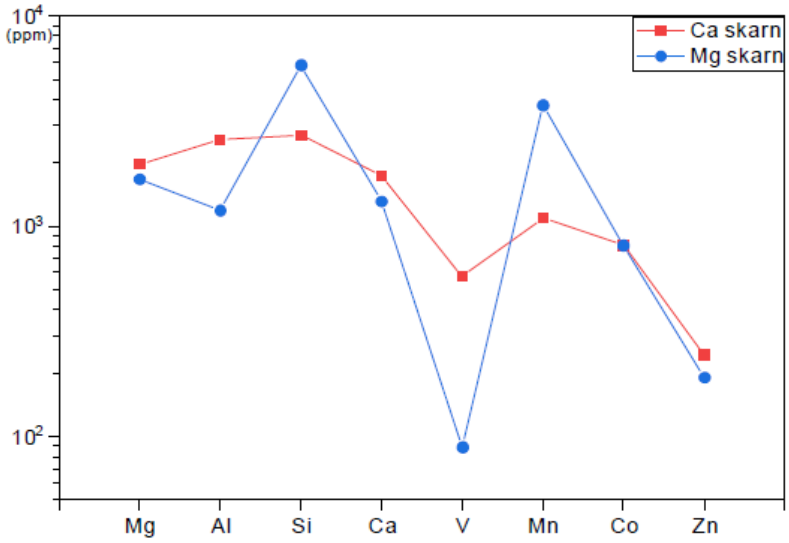

Figure 4. Average EPMA element contents of magnetite from calcic and magnesian skarns.

3.2. PLS-DA Results of Different Mineralization Types of Skarn Deposits

The partial least squares-discriminant analysis is used to examine whether the chemical compositions of magnetite could reflect the mineralization types of skarn deposits and to identify the most important discriminant elements. Figure 5 shows the PLS-DA results of the EPMA data. Magnetite from Fe skarn deposits can be roughly separated from that of Cu-Fe-Pb-Zn, Fe-Co-Bi-Ag, Fe-Cu, Fe-Zn, and Fe-Pb-Zn skarn deposits by t_1 due to a positive correlation with Si, Al, and Ti for the former (Figure 5a,b). In the t_2-t_3 score plot, magnetite from Fe-Zn skarn deposits can be distinguished from other mineralization types due to a positive correlation with Al and Mn (Figure 5c,d). The score contribution diagram shows that magnetite from the Cu-Fe-Pb-Zn skarn deposits has a relatively high Mn content compared to the average of the EPMA dataset (Figure 5e). Magnetite from the Fe skarn deposits has higher Al and Si contents and lower Mg and Mn contents than the other mineralization types (Figure 5f). Magnetite from the Fe-Co-Bi-Ag, Fe-Cu, and Fe-Zn-Pb skarn deposits shows a relative enrichment of Mg but with various enrichment degrees (Figure 5g,h,j), whereas magnetite from the Fe-Zn skarn deposit is characterized by a relatively high Mn content and low Si content (Figure 5i). The VIP plot shows that Mg in magnetite is important for discriminating between Fe, Fe-Co-Bi-Ag, Fe-Cu, and Fe-Zn-Pb deposits, whereas Mn is important in separating Cu-Fe-Pb-Zn, Fe-Zn, and Fe-Zn-Pb deposits (Figure 5k). Aluminum is an important discriminant element for all mineralization types. Silicon is only important to distinguish the Cu-Fe-Pb-Zn skarn deposit. Titanium is not important in the discrimination.

The relationship between elements and mineralization types based on the PLS-DA of LA-ICP-MS data is shown in Figure 6. Magnetite from Fe-Sn, Fe-Zn, and W-Mo-Pb-Zn-Fe-Cu skarn deposits can be roughly separated from that of other skarn deposits by t_1 due to positive correlation with Mn, Zn, and Sn for the former (Figure 6a–d). In the t_1-t_2 score plot, magnetite from the Fe-Au skarn deposit can be separated due to a positive correlation with Cr and Ga, whereas magnetite from the Fe-Cu skarn deposit can be separated because of a positive correlation with Mg and Co (Figure 6a,b). The score contribution diagram shows that magnetite from the Cu-Fe-Au and Fe-Au skarn deposits has relatively high Ga and Cr contents and low Mg and Mn contents but with various enrichment degrees (Figure 6e,g). Magnetite from the Fe skarn deposit is rich in Ti, V, and Co but depleted in Sn (Figure 6f). Magnetite from the Fe-Cu skarn deposit has higher Mg and Co contents and lower Cr and Ga contents than other mineralization types (Figure 6h). Magnetite from the Fe-Mo skarn deposit has relatively a high Mn content and low Ga content compared to the average of the LA-ICP-MS dataset (Figure 6i). Magnetite from Fe-Sn, Fe-Zn, and W-Mo-Pb-Zn-Fe-Cu skarn deposits shows the relative enrichment of Mn, Zn, and Sn and the depletion of V (Figure 6j,k,m), whereas magnetite from the Fe-Zn-Pb skarn deposit is characterized by relatively high Mn and Si contents and low Co, Zn, and Sn contents (Figure 6l). The VIP diagram indicates that Mg, Ti, V, Mn, Co, Zn, Ga, and Sn are important discriminant elements for different mineralization types (Figure 6n). Chromium in magnetite is only important for discriminating Fe-Au and Fe-Cu deposits, whereas Al, Si, Ca, and Ni are not important in the discrimination.

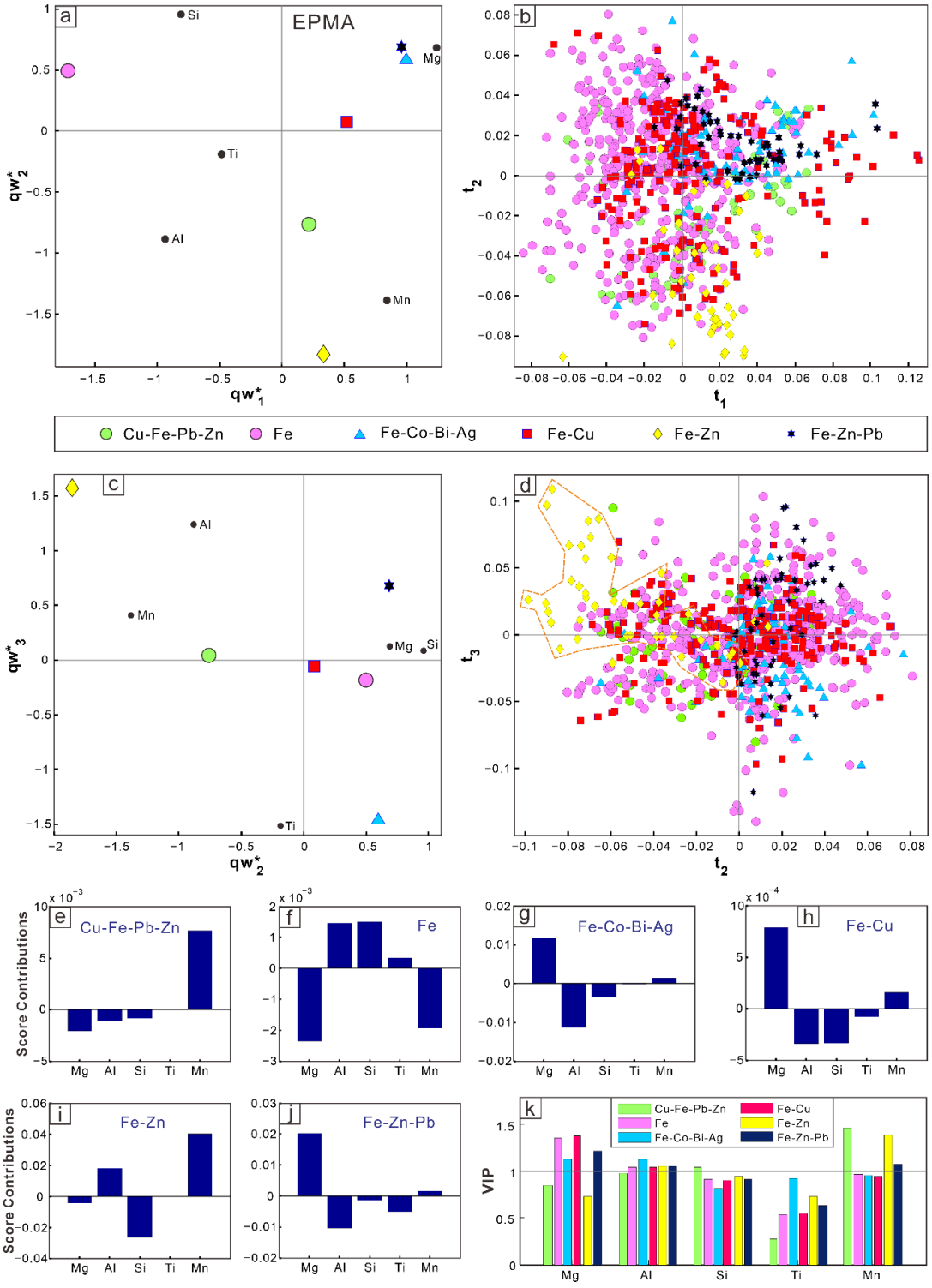

Figure 5. PLS-DA results of the EPMA data of magnetite. (**a**) The first and second loading plots show correlations among the element variables and mineralization types of skarn deposits. (**b**) The first and second score plots show the distribution of individual analyses of magnetite in the latent variable space defined by qw^*_1-qw^*_2 in (**a**). (**c**) The second and third loading plots show correlations among the element variables and mineralization types. (**d**) The second and third score plots show the distribution of individual analyses of magnetite in the latent variable space defined by qw^*_2-qw^*_3 in (**c**). (**e**–**j**) Score contribution plots for different mineralization types of skarn deposits. (**k**) Importance projection plot variance for the elements. The gray line marks the VIP value equal to 1.

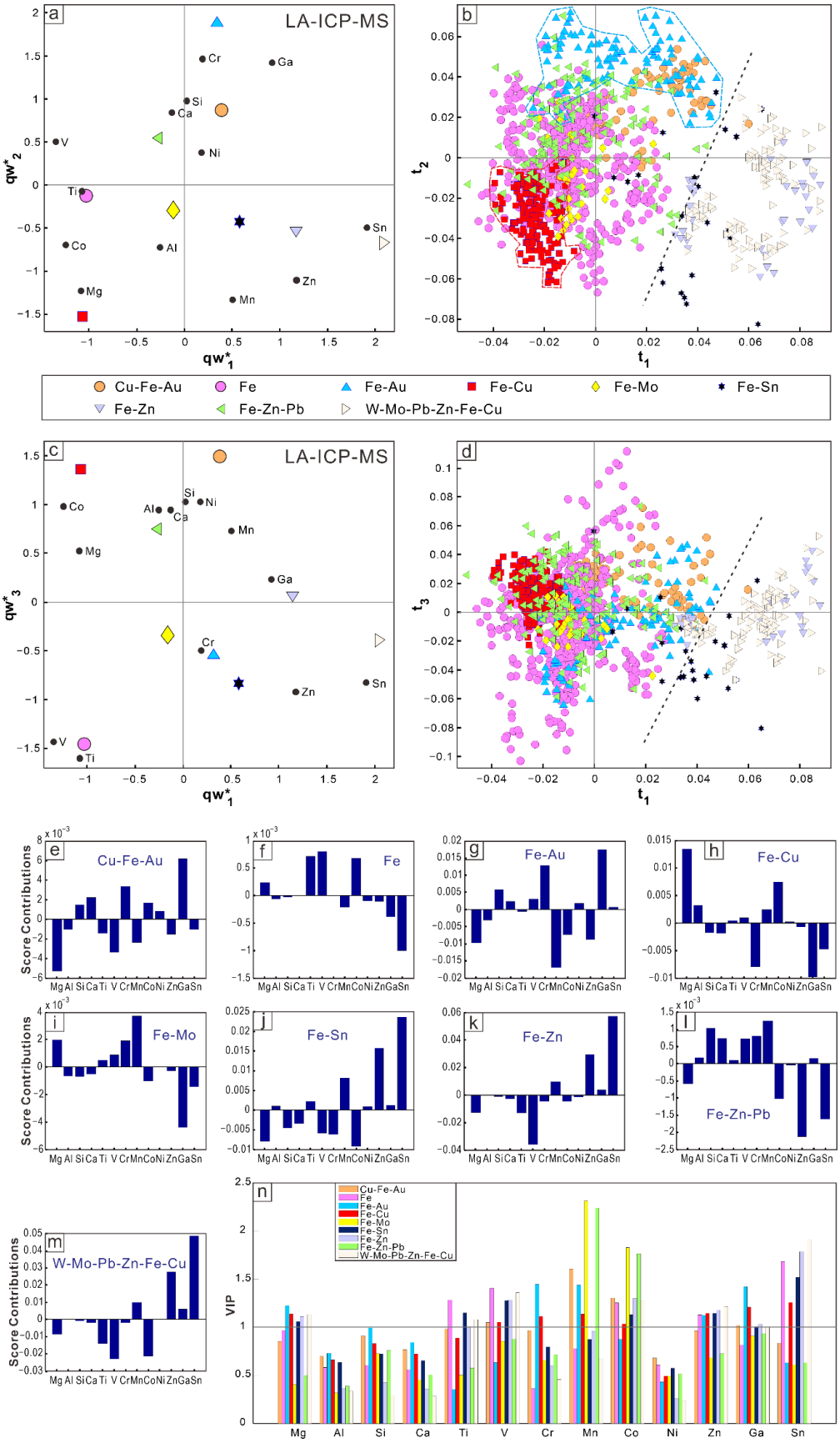

Figure 6. The PLS-DA results of LA-ICP-MS data of magnetite. (**a**) The first and second loading plots show correlations among the element variables and mineralization types. (**b**) The first and

second score plots show the distribution of individual analyses of magnetite in the latent variable space defined by qw^*_1-qw^*_2 in (**a**). (**c**) The first and third loading plots show correlations among the element variables and mineralization types. (**d**) The first and third score plots show the distribution of individual analyses of magnetite in the latent variable space defined by qw^*_1-qw^*_3 in (**c**). (**e**–**m**) Score contribution plots for different mineralization types of skarn deposits. (**n**) Important projection plot variance for the elements. The gray line represents the VIP value of 1.

4. Discussion

4.1. Factors for Variation in Chemistry of Skarn Magnetite

The factors affecting the chemical composition of hydrothermal magnetite are summarized as follows: (1) the concentration of the element in the hydrothermal fluids, (2) the temperature and oxygen fugacity, (3) whether other minerals that crystallize at the same time compete for the element, and (4) the re-equilibrium process [6,15–17]. In addition, the fluid–rock interaction is another important controlling factor for trace elements of magnetite in the skarn system [6,9,18].

4.1.1. Intrusive Compositions

A previous study illustrated the relationship between intrusive compositions and mineralization types of skarn deposits [2]. It is found that the intrusions associated with Fe and Au skarns have lower Si or K contents and a higher Mg content than the intrusions associated with the Sn and Mo skarns, which indicates that the magmatic evolutional degree of related intrusions of the Sn and Mo skarn deposits is higher than that of the Fe and Au skarn deposits [2]. Several researchers also concluded that the associated components of the Fe skarn deposit is directly related to the acidity of the intrusive rocks [19]. With the change of the magmatic rocks from intermediate-basic, intermediate, intermediate-acidic to acidic, the mineralization types change from Fe to Fe-Cu-Co, Fe-Sn-Zn, and Fe-Sn-Wo-Mo polymetallic assemblages [19]. For the EPMA data, we found that magnetite from Fe deposits has a higher Si content than the magnetite from Fe-Cu and Fe-Zn polymetallic deposits (Figure 3a), whereas for LA-ICP-MS data, there is no such rule (Figure 3b). This is inconsistent with the previous results that the intrusive compositions of a single Fe deposit were more basic, indicating that the Si content of magnetite cannot directly reflect the composition of the intrusions and further reflects that Si in magnetite is mainly controlled by fluid composition.

4.1.2. Fluid–Rock Interaction

Magnesian and calcic skarns can be used to describe the dominant composition of the protolith and resulting skarn minerals [3]. Hydrothermal magnetite from magnesian skarns is relatively rich in Mg and Mn and depleted in Al, Ti, Cr, Co, Ni, and Ga, whereas that from calcic skarns has relatively high Mg, Al, Cr, Mn, Co, Ni, and Zn and low Sn contents [6]. In terms of the average composition, magnetite from calcic skarns is relatively rich in Al and V, whereas magnetite from magnesian skarns is relatively rich in Si and Mn (Figure 4). The relative enrichment of Al in calcic skarns and Mn in magnesian skarns is consistent with a previous study [6]. This indicates that the country rock of magnesian or calcic carbonate rocks has some effect on the chemical composition of magnetite.

The fluid–rock interaction can have a significant effect on the composition of skarn magnetite, especially the elements such as Mg and Mn in magnetite [1,3]. In general, magmatic fluids from granites are rich in Si, Al, Fe, W, Na, K, F, and Cl [20], while carbonate surrounding rocks are rich in Ca, Mn, and Mg. The plot of (Si + Al)/(Mg + Mn) vs. Mg+Mn was proposed to distinguish between magnetite with various fluid/rock ratios in skarn systems [18]. The decreasing (Si + Al)/(Mg + Mn) value and increasing Mg + Mn content for magnetite from endoskarn to exoskarn indicate the decreasing fluid/carbonate rock ratios [18]. For the EPMA data, magnetite from Fe and Fe-Cu skarn deposits has relatively high (Si + Al)/(Mg + Mn) and low Mg+Mn contents (Figure 7a), while, for LA-ICP-MS data, magnetite from Fe-Au skarn deposits has relatively high (Si + Al)/(Mg + Mn) and

low Mg+Mn contents (Figure 7b), indicating a stronger degree of fluid participation for these mineralization types.

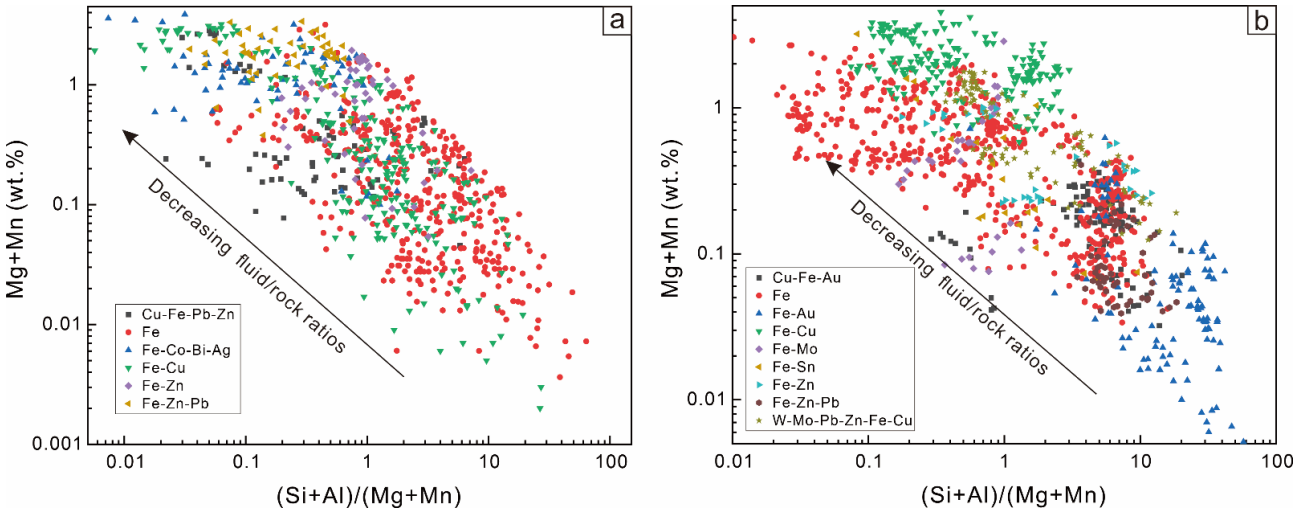

Figure 7. The plot of the EPMA (**a**) and LA-ICP-MS data (**b**) of magnetite in the (Si + Al)/(Mg + Mn) vs. Mg + Mn diagram proposed by Hu et al. (2014) [18]. The black arrows mean decreasing fluid/rock ratios.

4.1.3. Temperature

Temperature has a great influence on the partition coefficient. The data provided by Nadoll et al. (2014) [6] showed that the trace element content of hydrothermal magnetite with a lower temperature is generally lower, while that of high-temperature hydrothermal porphyries and skarn magnetite is relatively high. Since the Ti content in magnetite has a positive correlation with the temperature [21], it can be used to preliminarily explore the relationship between the skarn mineralization type and temperature. For EPMA data, magnetite from Fe-Co-Bi-Ag and Fe-Zn deposits has a relatively high Ti content, which means that the mineralization temperature is higher (Figure 3a). For LA-ICP-MS data, magnetite from Fe-Cu and Fe-Sn deposits has a higher Ti content than those from a Fe-Zn deposit, indicating that the formation temperature of the former is possibly higher than the latter (Figure 3b). Researchers also found that the XMg (=Mg/(Mg + Fe^{tot})) of magnetite is strongly dependent on the temperature and can be formulated into an empirical geothermometer [22]. Therefore, for EPMA data, we try to use a magnetite Mg thermometer to estimate the temperatures of various mineralization types. The average formation temperatures of the Cu-Fe-Pb-Zn, Fe, Fe-Co-Bi-Ag, Fe-Cu, Fe-Zn, and Fe-Zn-Pb deposits are 707.7 °C, 638.3 °C, 821.3 °C, 743.8 °C, 644.6 °C, and 882.5 °C, respectively. It shows that Fe-Zn-Pb and Fe-Co-Bi-Ag deposits have higher temperatures than Cu-Fe-Pb-Zn, Fe, Fe-Cu, and Fe-Zn deposits, with similar results from the magnetite mean Ti thermometer. In addition, the Fe skarn deposit has the highest upper limit of Ti (Figure 3b), which is consistent with the oxy-exsolution of Fe-Ti-Al oxides from magnetite in some Fe skarn deposits [16].

4.1.4. Oxygen Fugacity

Previous studies have shown that oxygen fugacity is the main factor controlling the distribution of elements among oxides and silicates in the melt [23]. The content of variable valence element V in magnetite is sensitive to the changes of different oxygen fugacity conditions, because V usually preferentially binds to the magnetite structure at low-oxygen fugacity but becomes incompatible at high-oxygen fugacity due to its 5+ oxidation state [21,24]. Magnetite in the Fe, Fe-Cu, and Fe-Zn-Pb skarn deposits has a relatively high V content, while magnetite in the Fe-Zn, Cu-Fe-Au, and W-Mo-Pb-Zn-Fe-Cu deposits is relatively depleted in V (Figures 3b and 6k), which seems to indicate that the

oxygen fugacity condition of the former is lower than that of the latter. Several researchers have also explored the correlation between the mineralization types and iron oxidation of skarn-associated intrusions and demonstrated that Cu, Zn, and Mo skarn intrusions are more oxidized than Au and Sn skarn intrusions [2]. The inconsistent results between the oxygen fugacity of magnetite and related intrusions indicate that the oxygen fugacity is significantly changed from magmatic to hydrothermal processes.

4.1.5. Co-Crystallized Minerals

The existence of co-crystallizing sulfides will compete for siderophile and chalcophile elements in magnetite, such as Co, Ni, Zn, Pb, Mo, and Sn [25]. Cobalt and Ni are mainly enriched in pyrrhotite and pyrite, and Zn is mainly enriched in sphalerite, whereas Sn is relatively enriched in cassiterite and magnetite. Magnetite from the Fe-Au deposit is depleted in Co, and magnetite from the Fe-Mo deposit is depleted in Ni (Figure 3b). Considering that the associated minerals with magnetite of these two deposits are pyrrhotite and pyrite [26,27], the depletion of Co and Ni in magnetite is likely to be caused by co-crystallizing sulfides. The W-Mo-Pb-Zn-Cu-Fe deposit contains amounts of sphalerite, but Zn is enriched in magnetite from these deposits compared with the other mineralization types (Figure 3b), which indicates that magnetite crystallizes earlier than sphalerite, or the fluids are extremely enriched in Zn. Experimental studies have shown that even a trace concentration of Zn in magnetite indicates that Zn is highly enriched relative to Fe in chloride-rich hydrothermal fluids [28]. Therefore, Zn enrichment in magnetite from the W-Mo-Pb-Zn-Fe-Cu deposit, in spite of the competition with sphalerite, most likely reflects Zn-rich hydrothermal fluids.

4.2. Discrimination between Magnetite from Different Mineralization Types of Skarn Deposits

In order to understand the distribution of different mineralization types of skarn deposits, we plotted the average and individual analyses of EPMA and LA-ICP-MS data in the Ti + V vs. Ni/(Cr + Mn) and Ti + V vs. Ca + Al + Mn diagrams (Figures 8 and 9). These diagrams have proven to be very efficient in distinguishing skarn magnetite from other deposit types. It is shown that most of the data points are located in the skarn field, and a few of them are located in the IOCG and Porphyry fields adjacent to the skarn field (Figures 8d and 9d). This is consistent with the fact that some high-Ti magnetite is present in skarn deposits, especially Fe skarn deposits [16], which possibly results in higher total Ti and V contents. However, this diagram cannot be used to further distinguish magnetite from different mineralization types of skarn deposits due to the similar variations in terms of the Ni/(Cr + Mn) ratios and Ti + V and Ca + Al + Mn contents.

For magnetite EPMA data, only Fe-Zn skarn deposits can be distinguished from other skarn deposits by a PLS-DA. For magnetite LA-ICP-MS data, despite there being some superposition, we were able to distinguish the mineralization types such as Fe-Au, Fe-Cu, Fe-Sn, Fe-Zn, and W-Mo-Pb-Zn-Fe-Cu of the skarn deposits. Based on the PLS-DA results, Mg, Al, Ti, V, Mn, Co, Zn, Ga, and Sn were identified as the most important elements for discriminating different mineralization types (Figures 5k and 6n). As shown in Figures 8 and 9, the total contents of Ti+V are not able to separate different mineralization types, and these two elements were not used to construct a new diagram. As shown in Figure 7, magnetite from different mineralization types is partly separated due to differences in the Mg+Mn contents. Different from the chalcophile behavior of Co and Zn, Ga is a lithophile element, and its content in magnetite is not affected by the crystallization of sulfides. Tin is concentrated more in magnetite than in any sulfide mineral, which implies that a Sn–O bond is perhaps more favorable than a Sn–S bond [25]. Based on the above considerations, a binary diagram of Mg+Mn vs. Ga+Sn is proposed to distinguish different types of skarn deposits (Figure 10). It is shown that Fe-Au, Fe-Cu, Fe-Mo, Fe-Zn, and W-Mo-Pb-Zn-Fe-Cu skarn deposits can be well-distinguished, in spite of the minor overlap between the Cu-Fe-Cu, Fe, and Fe-Zn-Pb skarn deposits. The reliability of the diagram still needs more data to be verified.

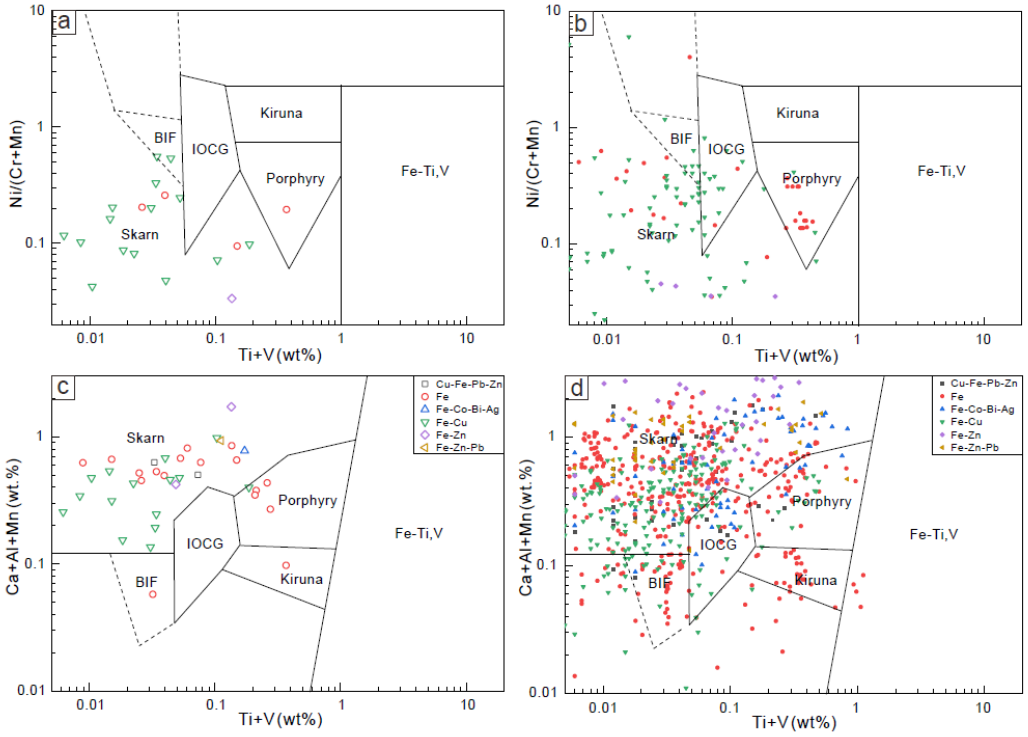

Figure 8. Plot of the EPMA average contents (**a**,**c**) and individual analyses (**b**,**d**) of magnetite in the Ti+V vs. Ni/(Cr+Mn) and Ti+V vs. Ca+Al+Mn diagrams proposed by Dupuis and Beaudoin (2011) [5]. BIF = banded iron formation, Skarn = Fe-Cu skarn deposits, IOCG = iron oxide copper gold deposits, Porphyry = porphyry Cu deposits, Kiruna = Kiruna apatite magnetite deposits, and Fe-Ti, V = magmatic Fe-Ti oxide deposits.

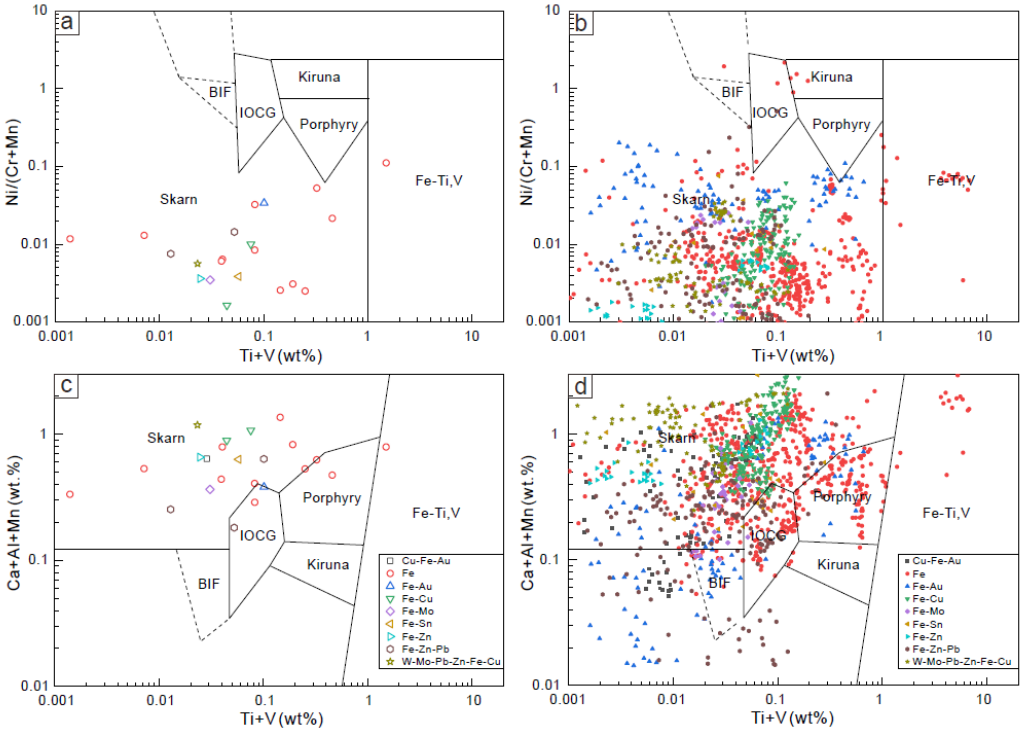

Figure 9. Plot of the average LA-ICP-MS content (**a**,**c**) and individual analyses (**b**,**d**) of magnetite in the Ti+V vs. Ni/(Cr+Mn) and Ti+V vs. Ca+Al+Mn diagrams proposed by Dupuis and Beaudoin (2011) [5]. The abbreviations are the same as those in Figure 8.

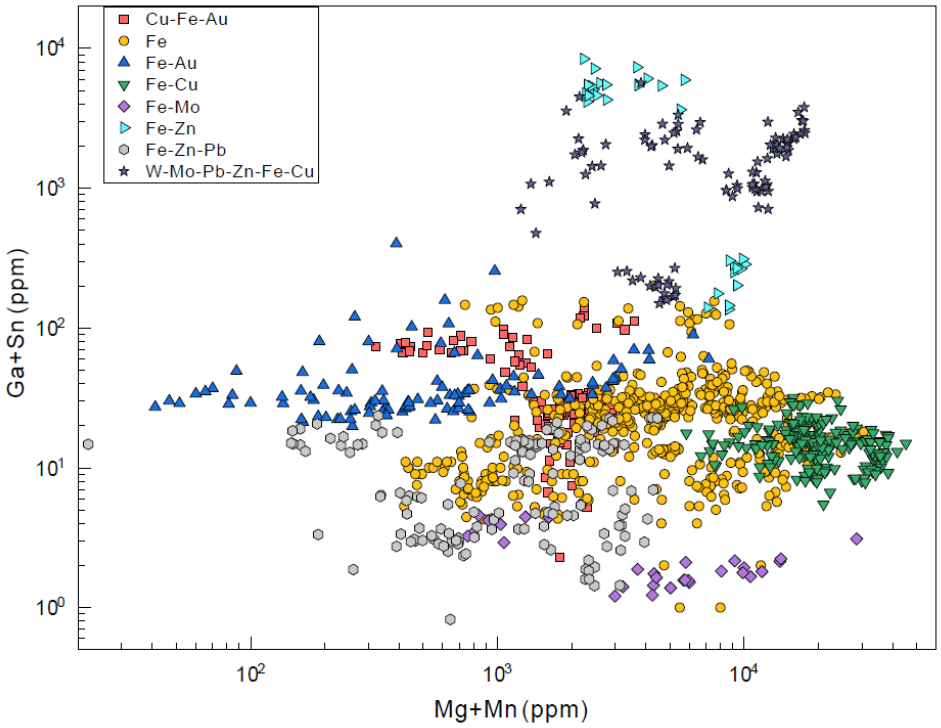

Figure 10. Plot of Mg+Mn vs. Ga+Sn to discriminate magnetite from different mineralization types of skarn deposits. The data points represent individual LA-ICP-MS analyses.

5. Conclusions

In this work, we used PLS-DA to investigate the relationship between magnetite chemistry and mineralization types of skarn deposits. For magnetite EPMA data, only the Fe-Zn skarn deposit can be distinguished from other skarn deposits. For magnetite LA-ICP-MS data, despite there being some superposition, mineralization types such as Fe-Au, Fe-Cu, Fe-Sn, Fe-Zn, and W-Mo-Pb-Zn-Fe-Cu skarn deposits can be distinguished. The identified discriminant elements are Mg, Al, Ti, V, Mn, Co, Zn, Ga, and Sn. The degree of fluid–rock interaction is a good index for distinguishing different mineralization types of skarn deposits. A plot of Mg + Mn vs. Ga + Sn was proposed to distinguish between different mineralization types, which provides a further discrimination for skarn deposits.

Supplementary Materials: The following supporting information can be downloaded at: https://www.mdpi.com/article/10.3390/min12050608/s1, Table S1: Summary of the basic information of the skarn deposits collected in this study. Table S2: Summary of the censored data of the magnetite trace elements analyzed by the EPMA and LA-ICP-MS [29–47].

Author Contributions: Conceptualization, X.H.; Data curation, H.X.; Formal analysis, H.X. and X.H.; Funding acquisition, X.H.; Investigation, H.X.; Methodology, X.H.; Software, X.H.; Writing—original draft, H.X.; Writing—review and editing, X.H., Y.M., H.T. and L.Q. All authors have read and agreed to the published version of the manuscript.

Funding: X.W.H. acknowledges the CAS Hundred Talents Program, Field Frontier Key Project of State Key Laboratory of Ore Deposit Geochemistry (202101), and National Natural Science Foundation of China (42173070).

Acknowledgments: The authors are very grateful to the reviewers for the work done.

Conflicts of Interest: The authors declare no conflict of interest.

References

1. Einaudi, M.T.; Meinert, L.D.; Newberry, R.J. Skarn deposits. *Econ. Geol.* **1981**, *75*, 317–391.
2. Meinert, L.D.; Dipple, G.M.; Nicolescu, S. World skarn deposits. In *Economic Geology 100th Anniversary Volume*; Hedenquist, J.W., Thompson, J.F.H., Goldfarb, R.J., Richards, J.P., Eds.; Society of Economic Geologists: Littleton, Colorado, 2005; pp. 299–336.
3. Meinert, L.D. Skarns and skarn deposits. *Geosci. Can.* **1992**, *19*, 145–162.
4. Chang, Z.; Shu, Q.; Meinert, L.D. Skarn Deposits of China. *SEG Spec. Publ.* **2019**, *22*, 189–234.
5. Dupuis, C.; Beaudoin, G. Discriminant diagrams for iron oxide trace element fingerprinting of mineral deposit types. *Miner. Depos.* **2011**, *46*, 1–17. [CrossRef]
6. Nadoll, P.; Angerer, T.; Mauk, J.L.; French, D.; Walshe, J. The chemistry of hydrothermal magnetite: A review. *Ore Geol. Rev.* **2014**, *61*, 1–32. [CrossRef]
7. Makvandi, S.; Ghasemzadeh-Barvarz, M.; Beaudoin, G.; Grunsky, E.C.; McClenaghan, M.B.; Duchesne, C.; Boutroy, E. Partial least squares-discriminant analysis of trace element compositions of magnetite from various VMS deposit subtypes: Application to mineral exploration. *Ore Geol. Rev.* **2016**, *78*, 388–408. [CrossRef]
8. Huang, X.-W.; Sappin, A.-A.; Boutroy, É.; Beaudoin, G.; Makvandi, S. Trace Element Composition of Igneous and Hydrothermal Magnetite from Porphyry Deposits: Relationship to Deposit Subtypes and Magmatic Affinity. *Econ. Geol.* **2019**, *114*, 917–952. [CrossRef]
9. Huang, X.-W.; Gao, J.-F.; Qi, L.; Meng, Y.-M.; Wang, Y.-C.; Dai, Z.-H. In-situ LA-ICP-MS trace elements analysis of magnetite: The Fenghuangshan Cu-Fe-Au deposit, Tongling, Eastern China. *Ore Geol. Rev.* **2016**, *72*, 746–759. [CrossRef]
10. Zhao, L.; Zhang, Y.; Shao, Y.; Li, H.; Ahmad Shah, S.; Zhou, W. Using garnet geochemistry discriminating different skarn mineralization systems: Perspective from Huangshaping W-Mo-Sn-Cu polymetallic deposit, South China. *Ore Geol. Rev.* **2021**, *138*, 104412. [CrossRef]
11. Tian, Z.-D.; Leng, C.-B.; Zhang, X.-C.; Zafar, T.; Zhang, L.-J.; Hong, W.; Lai, C.-K. Chemical composition, genesis and exploration implication of garnet from the Hongshan Cu-Mo skarn deposit, SW China. *Ore Geol. Rev.* **2019**, *112*, 103016. [CrossRef]
12. Huang, X.W.; Boutroy, E.; Makvandi, S.; Beaudoin, G.; Corriveau, L.; De Toni, A.F. Trace element composition of iron oxides from IOCG and IOA deposits: Relationship to hydrothermal alteration and deposit subtypes. *Miner. Depos.* **2019**, *54*, 525–552. [CrossRef]
13. De Iorio, M.; Ebbels, T.; Stephens, D. Statistical Techniques in Metabolic Profiling. *Handb. Stat. Genet.* **2007**, *1*, 347–373.
14. Wold, S.; Sjostrom, M.; Eriksson, L. PLS-regression: A basic tool of chemometrics. *Chemom. Intell. Lab. Syst.* **2001**, *58*, 109–130. [CrossRef]
15. Dare, S.A.S.; Barnes, S.-J.; Beaudoin, G.; Méric, J.; Boutroy, E.; Potvin-Doucet, C. Trace elements in magnetite as petrogenetic indicators. *Miner. Depos.* **2014**, *49*, 785–796. [CrossRef]
16. Hu, H.; Lentz, D.; Li, J.-W.; McCarron, T.; Zhao, X.-F.; Hall, D. Reequilibration processes in magnetite from iron skarn deposits. *Econ. Geol.* **2015**, *110*, 1–8. [CrossRef]
17. Huang, X.-W.; Beaudoin, G. Textures and Chemical Compositions of Magnetite from Iron Oxide Copper-Gold (IOCG) and Kiruna-Type Iron Oxide-Apatite (IOA) Deposits and Their Implications for Ore Genesis and Magnetite Classification Schemes. *Econ. Geol.* **2019**, *114*, 953–979. [CrossRef]
18. Hu, H.; Li, J.-W.; Lentz, D.; Ren, Z.; Zhao, X.-F.; Deng, X.-D.; Hall, D. Dissolution-reprecipitation process of magnetite from the Chengchao iron deposit: Insights into ore genesis and implication for *in-situ* chemical analysis of magnetite. *Ore Geol. Rev.* **2014**, *57*, 393–405. [CrossRef]
19. Li, C.; Zhou, X.; Zhao, F.; Liu, Z. Summarizing on the associated mineral characteristics and comprehensive recovery status of skarn iron deposits. *Land Resour. Her.* **2020**, *17*, 31–35. (In Chinese)
20. Tosdal, R.M.; Dilles, J.H.; Cooke, D.R. From Source to Sinks in Auriferous Magmatic-Hydrothermal Porphyry and Epithermal Deposits. *Elements* **2009**, *5*, 289–295. [CrossRef]
21. Toplis, M.J.; Carroll, M.R. An experimental study of the influence of oxygen fugacity on Fe-Ti oxide stability, phase relations, and mineral-melt equilibria in ferro-basaltic systems. *J. Petrol.* **1995**, *36*, 1137–1170. [CrossRef]
22. Canil, D.; Lacourse, T. Geothermometry using minor and trace elements in igneous and hydrothermal magnetite. *Chem. Geol.* **2020**, *541*, 119576. [CrossRef]
23. Frost, B.R. Introduction to oxygen fugacity and its petrologic importance. In *Oxide Minerals: Petrologic and Magnetic Significance*; Lindsley, D.H., Ed.; Reviews in Mineralogy; Mineralogical Society of America: Chantilly, VA, USA, 1991; Volume 25, pp. 1–9.
24. Toplis, M.J.; Corgne, A. An experimental study of element partitioning between magnetite, clinopyroxene and iron-bearing silicate liquids with particular emphasis on vanadium. *Contrib. Mineral. Petrol.* **2002**, *144*, 22–37. [CrossRef]
25. Dare, S.A.S.; Barnes, S.-J.; Beaudoin, G. Variation in trace element content of magnetite crystallized from a fractionating sulfide liquid, Sudbury, Canada: Implications for provenance discrimination. *Geochim. Cosmochim. Acta* **2012**, *88*, 27–50. [CrossRef]
26. Sun, X.; Lin, H.; Fu, Y.; Li, D.; Hollings, P.; Yang, T.; Liu, Z. Trace element geochemistry of magnetite from the giant Beiya gold-polymetallic deposit in Yunnan Province, Southwest China and its implications for the ore forming processes. *Ore Geol. Rev.* **2017**, *91*, 477–490. [CrossRef]
27. Wang, C.-M.; Zhang, L.; Tang, H.-S.; Chen, H.-Y.; Li, X.-L.; Zheng, Y.; Li, D.-F.; Fang, J.; Dong, L.-H.; Qu, X. Genesis of the Kaladawan Fe-Mo ore field in Altyn, Xinjiang, China: Constraints from mineralogy and geochemistry. *Ore Geol. Rev.* **2017**, *81*, 587–601. [CrossRef]

28. Ilton, E.S.; Eugster, H.P. Base metal exchange between magnetite and a chloride-rich hydrothermal fluid. *Geochim. Cosmochim. Acta* **1989**, *53*, 291–301. [CrossRef]
29. Hu, X.; Chen, H.; Zhao, L.; Han, J.; Xia, X. Magnetite geochemistry of the Longqiao and Tieshan Fe-(Cu) deposits in the Middle-Lower Yangtze River Belt: Implications for deposit type and ore genesis. *Ore Geol. Rev.* **2017**, *89*, 822–835. [CrossRef]
30. Liu, Y.N.; Fan, Y.; Zhou, T.F.; Xiao, X.; White, N.C.; Thompson, J.; Hong, H.L.; Zhang, L.J. Geochemical characteristics of magnetite in Longqiao skarn iron deposit in the Middle-Lower Yangtze Metallogenic Belt, Eastern China. *Miner. Deposita* **2019**, *54*, 1229–1242. [CrossRef]
31. Xie, Q.; Zhang, Z.; Hou, T.; Jin, Z.; Santosh, M. Geochemistry and oxygen isotope composition of magnetite from the Zhangmatun deposit, North China Craton: Implications for the magmatic-hydrothermal evolution of Cornwall-type iron mineralization. *Ore Geol. Rev.* **2017**, *88*, 57–70. [CrossRef]
32. Li, G. Iron Ore Deposits in the Eastern Tianshan Orogenic Belt (China): The Magnetite-Skarn-Magmatism Association. Ph.D. Thesis, University of Orleans, Orléans, France, 2012.
33. Yang, Y.-L.; Ni, P.; Pan, J.-Y.; Wang, G.-G.; Xu, Y.-F. Constraints on the mineralization processes of the Makeng iron deposit, eastern China: Fluid inclusion, H-O isotope and magnetite trace element analysis. *Ore Geol. Rev.* **2017**, *88*, 791–808. [CrossRef]
34. Huang, X.-W.; Zhou, M.-F.; Beaudoin, G.; Gao, J.-F.; Qi, L.; Lyu, C. Origin of the volcanic-hosted Yamansu Fe deposit, Eastern Tianshan, NW China: Constraints from pyrite Re-Os isotopes, stable isotopes, and in situ magnetite trace elements. *Miner. Deposita* **2018**, *53*, 1039–1060. [CrossRef]
35. Neumann, E.-R.; Svensen, H.H.; Polozov, A.G.; Hammer, Ø. Formation of Si-Al-Mg-Ca-rich zoned magnetite in an end-Permian phreatomagmatic pipe in the Tunguska Basin, East Siberia. *Miner. Deposita* **2017**, *52*, 1205–1222. [CrossRef]
36. Zhao, W.W.; Zhou, M.-F. In-situ LA-ICP-MS trace elemental analyses of magnetite: The Mesozoic Tengtie skarn Fe deposit in the Nanling Range, South China. *Ore Geol. Rev.* **2015**, *65*, 872–883. [CrossRef]
37. Hu, H.; Li, J.-W.; Harlov, D.E.; Lentz, D.R.; McFarlane, C.R.; Yang, Y.-H. A genetic link between iron oxide-apatite and iron skarn mineralization in the Jinniu volcanic basin, Daye district, eastern China: Evidence from magnetite geochemistry and multi-mineral U-Pb geochronology. *Geol. Soc. Am. Bull.* **2019**, *132*, 899–917. [CrossRef]
38. Canil, D.; Grondahl, C.; Lacourse, T.; Pisiak, L.K. Trace elements in magnetite from porphyry Cu-Mo-Au deposits in British Columbia, Canada. *Ore Geol. Rev.* **2016**, *72*, 1116–1128. [CrossRef]
39. Sun, W.A.; Yuan, F.; Jowitt, S.M.; Zhou, T.F.; Liu, G.X.; Li, X.H.; Wang, F.Y.; Troll, V.R. In situ LA-ICP-MS trace element analyses of magnetite: Genetic implications for the Zhonggu orefield, Ningwu volcanic basin, Anhui Province, China. *Miner. Deposita* **2019**, *54*, 1243–1264. [CrossRef]
40. Wang, M.; Wang, W.; Liu, K.; Michalak, P.P.; Wei, K.; Hu, M. In-situ LA-ICP-MS trace elemental analyzes of magnetite: The Tieshan skarn Fe-Cu deposit, Eastern China. *Geochemistry* **2017**, *77*, 169–181. [CrossRef]
41. Duan, S.; Zhang, Z.; Jiang, Z.; Zhao, J.; Zhang, Y.; Li, F.; Tian, J. Geology, geochemistry, and geochronology of the Dunde iron-zinc ore deposit in western Tianshan, China. *Ore Geol. Rev.* **2014**, *57*, 441–461. [CrossRef]
42. Wang, X.; Wei, W.; Lv, X.; Fan, X.; Wang, S. Stanniferous magnetite composition from the Haobugao skarn Fe-Zn deposit, southern Great Xing'an Range: Implication for mineral depositional mechanism. *Geol. J.* **2018**, *53*, 1823–1839. [CrossRef]
43. Ding, T.; Ma, D.; Lu, J.; Zhang, R. Magnetite as an indicator of mixed sources for W-Mo-Pb-Zn mineralization in the Huangshaping polymetallic deposit, southern Hunan Province, China. *Ore Geol. Rev.* **2018**, *95*, 65–78. [CrossRef]
44. Chen, F.; Deng, J.; Wang, Q.; Huizenga, J.M.; Li, G.; Gu, Y. LA-ICP-MS trace element analysis of magnetite and pyrite from the Hetaoping Fe-Zn-Pb skarn deposit in Baoshan block, SW China: Implications for ore-forming processes. *Ore Geol. Rev.* **2020**, 103309. [CrossRef]
45. Li, D.-F.; Chen, H.-Y.; Hollings, P.; Zhang, L.; Sun, X.-M.; Zheng, Y.; Xia, X.-P.; Xiao, B.; Wang, C.-M.; Fang, J. Trace element geochemistry of magnetite: Implications for ore genesis of the Talate skarn Pb-Zn (-Fe) deposit, Altay, NW China. *Ore Geol. Rev.* **2018**, *100*, 471–482. [CrossRef]
46. Yi, L.; Gu, X.; Lu, A.; Liu, J.; Lei, H.; Wang, Z.; Cui, Y.; Zuo, H.; Shen, C. Major and trace elements of magnetite from the Qimantag metallogenic belt: Insights into evolution of ore–forming fluids. *Acta Geol. Sin. (Engl. Ed.)* **2015**, *89*, 1226–1243.
47. Wang, C.; Shao, Y.; Zhang, X.; Dick, J.; Liu, Z. Trace Element Geochemistry of Magnetite: Implications for Ore Genesis of the Huanggangliang Sn-Fe Deposit, Inner Mongolia, Northeastern China. *Minerals* **2018**, *8*, 195. [CrossRef]